Variable effects of spatial resolution on modeling of nitrogen oxides

Chi Li[1], Randall V. Martin[1], Ronald C. Cohen[2,3], Liam Bindle[1], Dandan Zhang[1], Deepangsu Chatterjee[1], Hongjian Weng[4], and Jintai Lin[4]

[1]Department of Energy, Environmental Chemical Engineering, Washington University in St. Louis, St. Louis, MO, USA
[2]Department of Chemistry, University of California, Berkeley, Berkeley, CA, USA
[3]Department of Earth and Planetary Science, University of California, Berkeley, Berkeley, CA, USA
[4]Laboratory for Climate and Ocean-Atmosphere Studies, Department of Atmospheric and Oceanic Sciences, School of Physics, Peking University, Beijing, China

Correspondence: Chi Li (lynchlee90@gmail.com)

Abstract. The lifetime and concentration of nitrogen oxides (NO_x) are susceptible to non-linear production and loss, and consequently to the resolution of a chemical transport model (CTM). Here we use the GEOS-Chem CTM in its high performance implementation (GCHP) to investigate NO_x simulations over the eastern United States across a wide range of resolutions (13-181 km). Following increasing grid size, daytime surface NO_x concentrations over July 2015 generally decrease over the Great

5   Lakes (GL) region and increase over the Southern States (SS), yielding regional biases (181 km vs. 13 km) of -18% to 9%; meanwhile hydrogen oxide radicals (HO_x) increase over both regions, consistent with their different chemical regimes. Nighttime titration of ozone by surface nitric oxide (NO) was found to be more efficient at coarser resolutions, leading to longer NO_x lifetimes and higher surface concentrations of nitrogen dioxide (NO_2) over the GL in January 2015. The tropospheric NO_2 column density at typical afternoon satellite overpass time has spatially more coherent negative biases (e.g., -10% over

10   the GL) at coarser resolutions in July, which reversed the positive biases of surface NO_x over the SS. The reduced NO_x aloft (> 1km altitude) at coarser resolutions was attributable to the enhanced HO_x that intrudes into the upper troposphere. Application of coarse resolution simulations for interpreting satellite NO_2 columns will generally underestimate surface NO_2 over the GL and overestimate surface NO_2 over the SS in summer, while uniformly overestimating NO_x emissions over both regions. This study significantly broadens understanding of factors contributing to NO_x resolution effects, and the role of fine resolution to

15   accurately simulate and interpret NO_x and its relevance to air quality.

1 Introduction

Nitrogen oxides ($NO_x \equiv NO+NO_2$) have major roles in tropospheric chemistry and air quality. During daytime, NO_x interacts with hydrogen oxide radicals ($HO_x \equiv OH + HO_2$) and volatile organic compounds (VOCs) via photochemical reactions to affect formation of ozone and nitrate aerosols (e.g., Sillman, 1999; Thornton et al., 2002; Pusede et al., 2015; Zhu et al.,

20   2022). During nighttime, persistent NO_x emissions are the main chemical sink of ozone in urban areas (Zhang et al., 2004; Brown et al., 2006; Zakoura and Pandis, 2018), meanwhile the sequential formation of nitrate radical (NO_3) significantly alters nocturnal atmospheric oxidation capacity and secondary aerosols (Evans and Jacob, 2005; Brown and Stutz, 2012; Rollins et al., 2012). NO_x has strongly localized emissions (Miyazaki et al., 2017; Crippa et al., 2018; Beirle et al., 2019) and

relatively short lifetimes (Kenagy et al., 2018; Laughner and Cohen, 2019), which determine its strong spatial heterogeneity.

25   While such localization is advantageous for identifying and quantifying NO_x emissions using observations such as satellite nitrogen dioxide (NO_2) column density (e.g., Martin et al., 2006; Cooper et al., 2017; Goldberg et al., 2019; Laughner and Cohen, 2019; Wang et al., 2022), it poses as a challenge for chemical transport models (CTMs) to accurately represent the relevant production and loss processes at inter-urban scales (order 10 km) due to limited computational resources.

One outstanding issue is the resolution dependence of simulated NO_x lifetime (τ) (Charlton-Perez et al., 2009; Valin et al.,

30   2011), which is sensitive to NO_x abundance itself due to the interaction of NO_x with its own chemical loss (Laughner and Cohen, 2019; Shah et al., 2020) such as hydroxyl radical (OH) and ozone (e.g., Figure S1). Due to the stronger NO_x localization at higher resolution, systematic differences in the simulated τ and NO_x concentration at different resolutions were reported from modeled NO_x plumes of power plants, cities and ship emissions (Sillman et al., 1990; Charlton-Perez et al., 2009; Valin et al., 2011). Regional chemical transport modeling with more realistically distributed emissions was also performed to

35   examine how NO_x abundance changes with varying resolutions (Valin et al., 2011; Yamaji et al., 2014; Yan et al., 2016; Yu et al., 2016). The majority of these studies indicated increased τ and NO_x concentration at higher resolutions, and attributed it to the titration of OH by NO_x over sources (e.g., the right part of Figure S1). However, evidence (Laughner and Cohen, 2019; Jin et al., 2020; Zhu et al., 2022) has emerged that many cities across the United States (US) recently experienced the transition into the NO_x-limited regime following emission regulations, where stronger NO_x emissions actually promote HO_x

40   production and decrease τ (e.g., the left part of Figure S1). It is unclear how this change will update our understanding of the resolution dependency of simulated NO_x. Furthermore, nighttime effects were rarely studied possibly due to the prolonged τ and reduced NO_x localization, although significant spatial heterogeneity of nocturnal NO_x and ozone in urban environments were still noted (Zhang et al., 2004; Pan et al., 2017; Zakoura and Pandis, 2018), and long-term effects of changing NO_x on nighttime τ were also evident (Shah et al., 2020). Finally, retrieval of tropospheric NO_2 column density (Ω) from a growing

45   constellation of satellite instruments (e.g., OMI, TROPOMI, TEMPO, Sentinel-4, GEMS) offers observational information to constrain NO_x emissions across vast continental and global regions (Veefkind et al., 2012; Streets et al., 2013; Zoogman et al., 2017; Levelt et al., 2018; Timmermans et al., 2019; Kim et al., 2020); Existing studies have not separately discussed the resolution effects on Ω and on surface NO_x, which can potentially differ due to the vertically nonuniform spatial heterogeneity and species abundances.

50   This study uses a CTM across a wide range of resolutions to significantly enrich current understanding of resolution dependency of NO_x simulation. We find evidence over the eastern US that changes in simulated NO_x abundances at different resolutions are by no means uniform, but depend on factors such as chemical regimes, dominant processes, and vertical layering. This information urges the necessity to apply adequate resolution to simulate and interpret NO_x-relevant atmospheric chemistry and air quality issues.

2 Materials and methods

We use the GEOS-Chem model in its high performance implementation (GCHP, http://www.geos-chem.org, version 13.2.1, DOI: 10.5281/zenodo.5500718) to simulate NO_x and its relevant components over the eastern US.

GCHP is a grid-independent implementation of GEOS-Chem operating in a distributed-memory framework for massive parallelization (Long et al., 2015; Eastham et al., 2018). Chemical transport is simulated using a finite volume advection code (FV3) on a cubed-sphere grid (Putman and Lin, 2007). GCHP uses identical chemistry and physics modules as the standard GEOS-Chem code (GEOS-Chem Classic). A stretched-grid capability offers finer resolution over a user-specified domain of interest (Bindle et al., 2021). The model version used here (v13.2.1) features significant advances for performance and ease of use (Martin et al., 2022). The model is driven by the Goddard Earth Observation System Forward Processing (GEOS-FP) assimilated meteorological data with the native resolution of $0.25° \times 0.3125°$, from the NASA Global Modeling and Assimilation Office (GMAO). The GEOS-FP data is currently the finest resolution meteorology available for GCHP simulations for the simulation year, and was regridded to each simulation resolution, including the resolution (of 13 km) that is finer than $0.25° \times 0.3125°$. Although non-ideal, this capability as demonstrated by Bindle et al. (2021) will not significantly alter our interpretations focusing on discussing redistribution of NO_x emissions and chemical feedbacks, rather than effects from meteorology. Yan et al. (2016) showed that sub-coarse-grid emission-chemical variability dominantly contributed to the differences of simulated tropospheric chemistry between resolutions, overwhelming the effects from resolution of non-chemical factors such as meteorological data. Consistent with GEOS-FP, the atmosphere is vertically distributed into 72 layers (from surface to 0.01 hpa) following the hybrid sigma-pressure grid definition during the simulation. Boundary layer mixing is simulated with a non-local scheme (Lin and McElroy, 2010). The lowest layer is roughly 120 m thick, with mixing ratios of NO_x, HO_x and ozone that we refer to as the "surface concentrations".

We use the standard full-chemistry scheme of the GEOS-Chem model which is widely used to study air quality (Koplitz et al., 2016; Li et al., 2017; Shah et al., 2020; Gu et al., 2021). The scheme includes detailed gas-phase mechanisms of HO_x-NO_x-VOC-ozone chemistry (Bey et al., 2001; Mao et al., 2013; Sherwen et al., 2016) including heterogeneous uptake of reactive gases (McDuffie et al., 2018; Holmes et al., 2019) by the simultaneously simulated aerosols. Anthropogenic NO_x emissions are from EDGAR v5.0 at $0.1°$ resolution (Crippa et al., 2021), and speciated anthropogenic non-methane VOC emissions are from CEDS v2 (Hoesly et al., 2018). Open burning emissions are from GFED v4.1 (van der Werf et al., 2017). Although the latter two inventories have non-ideal ($0.5°$ and $0.25°$) resolutions due to availability, they are acceptable for our purpose of identifying the resolution dependence of NO_x. One favorable capability of the simulation is the pre-calculated offline dust, lightning NO_x, biogenic VOC (BVOC), soil NO_x and sea salt aerosol emissions (Murray et al., 2012; Weng et al., 2020; Meng et al., 2021), which avoids possible regional emission biases due to online calculations using meteorological fields at different resolutions, and the consequent interference on the interpretation of the results. All the emissions are handled by the HEMCO 3.0 module (Keller et al., 2014; Lin et al., 2021).

We conduct GCHP simulations for January (winter) and July (summer) of 2015, at six resolutions spanning the range of conventional global model capabilities (Table 1). The highest resolution (13 km) is close to the currently finest information

from emission inventories (0.1°) in global CTMs without downscaling, and the lowest resolution (181 km) remains widely used

90   in global and regional air quality studies (i.e. similar to 2°×2.5° resolution). For the three relatively coarser resolutions, we conduct global cubed-sphere simulations, while for resolutions < 50 km, we exploited the recently developed grid-stretching capability (Bindle et al., 2021) to greatly reduce the computational resource requirements. The stretched-grid configuration smoothly decreases the grid cell size towards the refined region of interest. We follow recommendations by Bindle et al. (2021) to choose moderate stretch factors (Table 1), ensuring that the lowest resolutions (i.e. on the antipode of the refined region)

95   remain finer than 300 km whilst achieving the substantially refined resolutions over the eastern US (Table 1, right).

Initial conditions on December 1, 2014 and June 1, 2015 are obtained from a 1-year spin-up run at C360 global cubed-sphere simulation using identical model version and inputs. These initial conditions resemble realistic global high-resolution ($\sim$25 km) distribution of NO_x-relevant species and their oxidants driven by the consistent emissions and chemistry used in this study, and were then regridded to drive the 2-month simulations at each resolution. The second month (January and July 2015)

100   from each simulation is used for the analysis to allow for further spin-up at each resolution. We archive the hourly average model outputs to enable the detailed discussion in the result section.

Figure 1a shows the study domain of interest (70–98°W and 26–48°N) and the emission ratio of isoprene to NO_x. The northern part of the domain comprises some of the most populous cities of the continent (e.g., New York, Toronto and Chicago), with strong and localized NO_x emissions as observed from space (Russell et al., 2012; Lu et al., 2015; Laughner and Cohen,

105   2019), ideal for investigating NO_x resolution dependence. The southern regime is characteristic of the strongest biogenic VOC (e.g., isoprene) emission rates across the US (Romer et al., 2016; Yu et al., 2016; Jin et al., 2020) that could affect the NO_x lifetime and its response to resolution.

To assess the implications for interpreting satellite observations of NO_2, we also apply monthly mean scattering weights (w) (Palmer et al., 2001) from the TROPOspheric Monitoring Instrument (TROPOMI) at its overpass time (UTC 19-21, namely

110   1-3 pm at central standard time (CST)) to calculate NO_2 line-of-sight (slant) column density (Ω_s). Comparing Ω_s with Ω enables investigation of effects of satellite sensitivity on the resolution dependency of NO_2 columnar abundances. TROPOMI is currently the only instrument with sufficient fine resolution to provide w information for all the investigated resolutions over the study domain. We assign every clear sky (i.e. geometric cloud fraction < 0.2) TROPOMI w in January or July of 2019 to the collocated grid cells of each resolution, to derive the monthly mean w distribution, which is then applied to the afternoon

115   mean NO_2 profiles in the same month of 2015 for each grid cell to calculate Ω_s.

In this study, all the regridding procedures between different resolutions are conducted using the conservative (surface area-weighted) algorithm (https://earthsystemmodeling.org/regrid/) in the Earth System Modeling Framework.

3   Results

3.1   Daytime resolution effects at surface in summer

120   Figure 1c shows the daytime (UTC 15-24, corresponding to CST 9-18) resolution effects of simulated surface NO_x concentrations over the eastern US in July 2015. At the finest resolution of 13 km (upper left), NO_x exhibits notable local enhancements

over cities and major industrial corridors due to its short lifetime (τ, several hours). Overall, the stronger emissions and agglomerate sources in the Great Lakes region (GL, green box) lead to higher NO_x levels than in the Southern States (SS, magenta box) where NO_x sources are relatively weaker and sparser. As the grid cell size increases to 22 km resolution, the NO_x level

125 shows overall decreases over emission centers and increases over nearby grids (by up to 1 ppb) relative to 13 km, an expected consequence due to dilution of emissions. However, systematic biases in predicted NO_x relative to 13 km resolution start to emerge especially further downwind and over the SS, reflecting the effects from the resolution-dependent τ. The biases relative to 13 km resolution become increasingly pronounced and regionally coherent as grid cells further enlarge. At the three coarse resolutions (> 50 km), a clear dipole of negative biases over the GL and positive biases over the SS becomes observable.

130 The opposite resolution effects of simulated NO_x over the GL and SS are summarized as regional mean biases in each panel of Figure 1c (e.g., -17.5% at 181 km over the GL), which are attributable to their corresponding chemical regimes. The GL in summer is characterized by stronger NO_x emissions and lower VOC emissions, while the opposite scenario prevails over the SS with strong BVOC sources, characterized partially by the distribution of isoprene/NO_x emission ratio in Figure 1a. Consequently, the NO_x sources in the GL tend to locate in the NO_x-saturated regime (Figure S1, right) where concentrated

135 NO_x levels at higher resolutions consume more OH and increase τ; Meanwhile over the SS, the relatively lower NO_x together with the enhanced VOC can reversely promote HO_x production at higher NO_x levels (NO_x-limited regime, Figure S1, left), thus higher resolution will introduce higher OH and lower τ. The lowered τ can be a result of directly scavenging NO_2 by the enhanced OH, and of indirectly sinking nitric oxide (NO) by the OH-promoted organic peroxy radicals (RO_2), an important NO_x sink pathway under low-NO_x and high-VOC environments (i.e. the SS) (Browne and Cohen, 2012; Perring et al., 2013;

140 Romer et al., 2016; Romer Present et al., 2020). As NO_x emissions continue to decrease, multiple lines of evidence suggest that NO_x sources widely across the United States have recently entered or are approaching the NO_x-limited regime (Laughner and Cohen, 2019; Jin et al., 2020; Koplitz et al., 2021; Jung et al., 2022; Zhu et al., 2022), especially over the SS since the 2010s (Jin et al., 2020; Koplitz et al., 2021; Zhu et al., 2022).

Figure 1b shows examples of daytime HO_x-NO_x relationships for 12 cities. We use HO_x to identify the regime represen-

145 tation since OH is unstable with a very short lifetime (~1s). HO_x and NO_x are anti-correlated over the GL (green labeled) while positively correlated over the SS (magenta labeled), consistently indicative of their different chemical regimes. The mean NO_x concentrations (circles) in Figure 1b thus roughly decrease over the GL and increase over the SS following the opposite changes in τ, as grid cell size increases (i.e. from magenta to brown circles). The mean HO_x biases within the $2° \times 2°$ windows above the cities are uniformly positive due to the opposite HO_x-NO_x associations over the GL and SS.

150 Unlike over the GL where the regional biases of surface NO_x gradually increase in magnitude following increasing grid cell sizes (Figure 1c, green numbers), the five resolutions > 13 km indicate small changes in the regional NO_x concentration across the SS (i.e. biases of 6.4-8.7%); namely, the systematic increase occurs primarily between 13 and 22 km resolutions (Figure 1c, magenta numbers). This observation can be related with the variation of spatial extent of chemical regimes and their effects on the NO_x biases during the course of the day. Figure S2 shows the resolution-dependence of simulated surface

155 NO_x separately for morning (left) and afternoon (right). Relative to the overall effects during daytime (Figure 1c), the NO_x-saturated regime (with negative NO_x biases at coarser resolution) has broader extent (e.g., intruding further into Tennessee) in

the morning hours, while the NO_x-limited regime (positive NO_x biases at coarser resolution) can significantly affect southern Ohio during the afternoon. The magnitudes of NO_x bias (e.g., 181 km vs. 13 km) are also enhanced over the GL in the morning (-27.1%) and over the SS in the afternoon (13.7%). These differences are consistent with the relative diurnal evolution of NO_x

160 (decreases since sunrise) and HO_x (accumulates and peaks after noon) abundances and the consequence on the dominant HO_x loss pathway (e.g., Ren et al., 2003; Ma et al., 2022). The inclusion of morning hours could therefore partially explain the relatively weaker resolution dependence in daytime NO_x over the SS.

Another potential cause of weaker sensitivity of simulated NO_x to resolution is the impacts from BVOC in addition to NO_x heterogeneity. Figure S3 shows that changing VOC reactivity mainly affects OH concentration and τ over the NO_x-

165 limited regime while has little effects on the NO_x-saturated regime, consistent with previous studies (Edwards et al., 2014; Laughner and Cohen, 2019; Zhu et al., 2022). Apart from increasing OH that decreases τ (Figure S3), decreasing VOC can also oppositely decrease the strength of the $NO-RO_2$ loss pathway and increase τ (Browne and Cohen, 2012). Nonetheless, both processes indicate increasing sensitivity of τ to VOC at low-NO_x environments (Romer et al., 2016; Laughner and Cohen, 2019; Romer Present et al., 2020). The SS feature strong BVOC emissions as well as strong spatial segregation of NO_x and

170 VOC sources (Yu et al., 2016; Travis et al., 2016), as reflected by lower isoprene/NO_x emission ratios in urban centers relative to its neighborhood in Figure 1a. Such segregation is reduced as the resolution lowers (e.g., Figure S4). The concurrent and usually opposite changes of NO_x (increases) and BVOC (decreases) emissions around NO_x sources at higher resolutions can jointly lead to the overall small changes among resolutions > 13 km. In summary, our simulations reveal that the predictability of actual resolution dependency of NO_x in the NO_x-limited regime is reduced due to the joint sensitivities to VOC.

175 ## 3.2 Nighttime resolution effects at surface in winter

Figure 2a shows surface NO_x concentration and its resolution dependence at nighttime (UTC 4-11 or CST 22-5) in January, 2015. With prolonged τ (~20 hours) as photochemistry ceases and OH becomes negligible, the wintertime and nighttime NO_x exhibits reduced spatial heterogeneity (e.g., Figure S5) relative to summertime and daytime in Figure 1c, and the resolution effects are thus also less pronounced (i.e. ≤5%). However, one characteristic phenomenon at nighttime that depends on resolu-

180 tion is the titration between NO and ozone (O_3), which is the main nighttime sink to each other in urban environments (Brown et al., 2006; Wang et al., 2006; Brown and Stutz, 2012; Kenagy et al., 2018; Shah et al., 2020). Figures 2b and 2c indicate that the titration between NO and O_3 at the surface is enhanced by enlarged grid cells, as both concentrations were near uniformly reduced (by ~50% and ~10%, respectively) across the domain. At coarser resolutions, the faster titration produces more NO_2, complemented by less efficient scavenging of NO_2 by the more titrated O_3 (Figure 2d). The resolution effect on surface NO_x

185 (Figure 2a) is thus jointly contributed by the opposite changes in NO (Figure 2b) and NO_2 (Figure 2d), the latter being more determinant due to its stronger contribution to total NO_x.

The faster titration efficiency at coarser resolution is driven by the spatial anti-correlation of NO and O_3, as demonstrated by Figure S6. Typical nighttime high-NO regions are coincident with low-O_3 locations at 13 km resolution (first row), a result of daytime O_3 formation suppression and nighttime O_3 titration (Jacob et al., 1995; Zhang et al., 2004; Jin et al., 2017; Yan et al.,

190 2018; Sicard et al., 2020; Li et al., 2022) over strong NO_x sources. This anti-correlation at fine resolution leads to inefficient

NO-O_3 reaction, which is to first-order proportional to their products, shown in the third column in Figure S6. By simply diluting their concentrations to larger grid cells (2rd-6th rows), the products of NO-O_3 from less anti-correlated concentrations are enhanced systematically. Consequently, there would also be faster production of N_2O_5 and nitrates, which were proposed by Zakoura and Pandis (2018) to explain the systematic overprediction of nitrate aerosols by CTMs at coarse resolution.

195   As the GL region has greater NO concentrations than the SS (Figure 2b), surface O_3 is more effectively titrated (Figure 2c), leading to increased NO_2 and NO_x concentrations (Figure 2d). Meanwhile over the SS, the NO_2 response is less pronounced due to the lower NO levels, and NO_2 exhibits reductions over certain locations at lower resolutions (Figure 2d), indicating that the excess O_3 can consume more NO_2 after titrating NO over these grids.

3.3   Seasonal and diel variation of relevant processes

200 Figure 3 summarizes the resolution effects of regional mean surface NO_x, HO_x and ozone, at different hours of the day. Over the GL, the strongest percentage biases of regional mean NO_x (mainly NO_2, Figure S7) at resolutions > 13 km occur at nighttime in January (up to 5%), and at daytime in July (up to -30%), revealing a pronounced seasonality of dominant mechanisms driving the resolution effects. This seasonality is driven by the stronger intensity and duration of daytime oxidant production in July (i.e. magenta lines for HO_x and O_3 in Figure 3); meanwhile the greater nighttime O_3 titration at coarser

205 resolution partially counteracts the daytime effects in July (i.e. reduces the percentage biases) and dominates in January.

The SS region has relatively stronger daytime resolution sensitivity that compensates the opposite nighttime effects on NO_2 in January (Figure S7), resulting in overall small changes in NO_x. In July, the resolution effects are again dominated by the daytime processes but in the NO_x-limited regime, which reverse the titration-driven opposite nighttime effects (more notable for HO_x and O_3). Unlike over the GL or in January, NO becomes remarkably determinant of the diel variation of NO_x biases

210 (Figure S7), reflecting the importance of the NO+RO_2 loss pathway on τ over the summer of the SS (Browne and Cohen, 2012; Perring et al., 2013; Romer et al., 2016; Romer Present et al., 2020). The small resolution dependence of the regional NO/NO_x biases at resolutions > 22 km again reflects the joint and compensating effects on NO_x lifetime from NO_x localization and VOC segregation (Section 3.1).

Overall, the daytime resolution effects driven by the involvement of NO_x in HO_x and O_3 production (Section 3.1) compete

215 with the nighttime effects driven by NO_x-O_3 titration (Section 3.2). The changing dominance of each mechanism during summer vs. winter, as well as during daytime and nighttime, leads to the characteristic seasonal and diel variation in Figure 3.

3.4   Vertically variable resolution effects

Figure 4 shows the resolution-dependent changes in regional mean daytime NO_x vertical profile in the lower troposphere (below 4 km). Uniform decreases in the simulated daytime NO_x following larger grid cells are apparent at > 1km altitude in

220 July, despite opposite changes over the two regions near surface (Figure 1). These vertically dependent responses are caused by the different vertical profiles of NO_x and HO_x (i.e. magenta lines). As NO_x mixing ratio decreases exponentially aloft while HO_x increases (in the GL) or remains relatively uniform (in the SS), HO_x becomes more abundant relative to NO_x at higher altitudes, meaning that τ is less sensitive to NO_x local concentrations even above strong NO_x sources. The enhanced oxidants

225 (ozone and HO_x) due to surface NO_x emission heterogeneity (Section 3.1) then vertically mixed to systematically enhance HO_x profile (Figure 4, right) and reduce τ and NO_x in these aloft layers. Therefore, both regions exhibit negative NO_x biases due to coarse resolution above 1 km, regardless of chemical regime.

Figure 5 shows the changes in nighttime vertical profile of NO_x and O_3 in January. Again, there are opposite vertical distributions of NO_x and its nighttime sink (ozone). Over the GL, although surface NO_x lifetime can be possibly prolonged at coarse resolution due to the faster titration of O_3 by NO (Section 3.2), NO quickly becomes insufficient to titrate the
230 increasing ozone at higher altitudes. Therefore, both NO_x species ultimately become affected by the resolution-dependent titration efficiency above 1 km (similar to the surface responses over the SS), leading to the negative biases in simulated NO_x, regardless of surface NO_x emission strength.

In summary, Figures 4 and 5 reveal that the resolution effects of τ at surface can differ from those at elevated altitudes, even over source regions. Such altitude-dependent responses will further affect interpretation of satellite-retrieved NO_2 columnar
235 properties, using model simulations at these resolutions.

3.5 Implications for satellite remote sensing applications

Satellite retrievals of NO_2 vertical column density (Ω) have been widely used to quantify and characterize spatiotemporal variation of NO_x abundances and sources. Here we evaluate the implications of the NO_x resolution dependency on two major applications—estimating surface NO_2 concentration and deriving NO_x emissions.
240 Figure 6 shows the simulated fraction of NO_2 abundance within the surface layer of GEOS-Chem relative to the whole troposphere, during Low Earth orbit (LEO) afternoon satellite overpass time. This surface fraction (F_s) is lower in summer than in winter, driven by stronger convection, lightning NO_x, and elevated boundary layer. F_s is also lower over the SS than the GL in July, due to relatively less NO_x emissions at surface and stronger lightning NO_x emissions in the upper troposphere (Murray et al., 2012; Silvern et al., 2019; Zhu et al., 2019). The changes of F_s following varying resolutions in general qualitatively
245 resemble these of surface NO_x (e.g., comparing Figure 6 with Figures 1c and Figure 2a). Overall, F_s has stronger biases in July than in January, lowered by 8% over the GL and enhanced by 7% over the SS at 181 km, relative to 13 km resolution. As F_s is a key parameter in estimating surface NO_2 concentration from satellite retrieved Ω (Lamsal et al., 2008; Cooper et al., 2020), directly applying the simulated NO_2 vertical profiles will propagate such resolution-dependent biases that also vary regionally and seasonally, as indicated in Figure 6.
250 Figure 7 shows the simulated tropospheric NO_2 vertical column density (Ω) and its resolution dependence during LEO afternoon overpass time, and Figure S8 shows the corresponding slant column density (Ω_s) after applying TROPOMI scattering weights. Relative to the surface biases (Figure 1c), the Ω and Ω_s differences show stronger regional uniformity, revealing overall increasingly negative biases with increasing grid size over both seasons and regions. For July and over the SS, the daytime columnar biases are reversed to be negative compared to the positive surface biases (e.g., Figure 7 vs. Figure 1c), driven by the
255 reversed responses at higher altitudes (Figure 4). This remarkable reversal of Ω biases (negative) vs. surface biases (positive) reinforces the need to include vertical profile information in correctly simulating NO_x columnar properties. Ω and Ω_s exhibit quantitatively consistent resolution dependence and its spatial distribution (Figure 7 vs. Figure S8), indicating that the changes

of vertical profile do not significantly alter the resolution dependency of satellite observed columnar abundances, compared to the direct effects from changing τ. Assuming NO_x emissions are locally related with NO_2 columns at coarse resolution will

260 result in similar magnitudes of overprediction (up to 10% and 7% over the GL and SS, respectively in July) of derived NO_x emissions to compensate the underestimated Ω to emission relationship, under an inverse modeling framework configured at each resolution, as shown in Figures 7 and S8.

4   Discussions and conclusions

The strong, and more importantly regionally variable, NO_x resolution dependences that we find in the lower troposphere

265 over the contemporary eastern US warrants care in interpreting coarse resolution NO_x simulations. We find that resolution-dependent NO_x biases are particularly large at the surface in summer, with variable effects seasonally, regionally, diurnally, and vertically, which also affect remote sensing observations interpreted with low resolution simulations. Existing literature about NO_x resolution dependencies in box models (Valin et al., 2011), in power plant (Sillman et al., 1990) and ship plumes (Charlton-Perez et al., 2009), and in CTMs (Wild and Prather, 2006; Yamaji et al., 2014; Yan et al., 2016) primarily discusses

270 the NO_x-saturated regimes; We find limited prior literature about the positive biases of NO_x over weak sources (i.e. in the NO_x-limited regime over the SS) in CTM simulations. The lack of similar prior reports reflects the chemical regime transition occurring in the recent ~10 years, while previously, typical point sources were predominantly in the NO_x-saturated regime. Attention to the NO_x-limited regime and its corresponding resolution effects is timely given declining NO_x emissions across the US with NO_x emission regulations. At the same time, the joint sensitivity to NO_x heterogeneity and concurrent VOC level

275 (Section 3.1) in the NO_x-limited regime will continue complicating its predictability, since NO_x and VOC can have various spatial co-variabilities (e.g., positively correlated where transportation-relevant VOC and NO_x both dominates) and regime-dependent effects on τ. Therefore, accurately capturing such regime difference and transition from CTM requires not only accurate emission inventories of NO_x and VOC, but also simulations at representative spatial scales that correctly distribute these emissions.

280 We found systematic resolution effects of nighttime NO-O_3 titration efficiency that can drive the NO_x biases over winter (Figure 2 and Section 3.2), as the anti-correlation between NO and O_3 implies faster reaction rates at coarser resolutions. In air quality modeling, many key reactions involve spatially correlated (e.g., co-emitted SO_2 and NO_2 to cause severe urban haze (Wang et al., 2020)) or segregated species (e.g., agricultural NH_3 and NO_x-formed HNO_3 for nitrate aerosol partitioning (Gu et al., 2021)). Like in this study, the segregated species will consume precursors and produce products more efficiently

285 at coarser resolutions, while collocated sources will experience opposite effects. Interpreting the evolution of relevant species and air pollution processes using CTM is therefore also preferable at the spatial scales that are representative of these sources, or should take this effect into account if performed on coarser scales.

Our detailed simulation of resolution effects at different altitudes (Figures 4 and 5) significantly enriched the understanding of resolution dependency of satellite columnar observations, in contrast to previous studies that neglected vertical layering.

290 The example of opposite resolution effect of Ω and surface NO_x (Figure 7 vs. Figure 1c) over the SS and July highlights the

necessity of realistic vertical profiling of NO_x and its chemical sinks. For two conventional applications of satellite retrieved Ω, namely estimation of surface NO_2 concentration and constraining NO_x emissions, we found that regionally and seasonally varying biases at the level of $\sim$10% due to adopting coarse model simulations ($\sim$200 km) are inevitable.

Overall, we conducted a comprehensive novel evaluation of NO_x resolution dependence using a CTM across a wide range
295 of resolutions (13-181 km) and scenarios (including nighttime, winter and higher altitudes). We found the strongest resolution effects in the summer and daytime (e.g., -18% for surface NO_x and -10% for columnar NO_2 over the Great Lakes), where and when the NO_x spatial heterogeneity is the strongest and its lifetime is the shortest (e.g., Figure S5). These systematic resolution dependences should be considered when constraining model parameters (e.g., emissions, reaction yields, removal rates, etc.) using ground- or satellite-based observations. In other words, relevant interpretations and conclusions by coarse
300 model simulations in previous studies are worth revisiting.

Although this study exploited state-of-science capabilities, biases with respect to resolutions finer than 13 km resolution likely exist considering the severely localized NO_x especially in summer (Valin et al., 2011; Larkin et al., 2017; Beirle et al., 2019). Following NO_x regulations in the US, the magnitudes of resolution effects are expected to continue decreasing as the enhancements over sources reduced relative to the background NO_x level (Russell et al., 2012; Jin et al., 2020; Qu et al.,
305 2021), and the requirements on resolution may diminish (e.g., partially reflected by the smaller effects over the SS relative to over the GL). Nonetheless, over developing areas where current NO_x emissions are stronger or are projected to increase, the resolution effects will be exacerbated, and applying finer-resolution simulations to accurately capture NO_x lifetime and budgets will be increasingly critical for air quality modeling applications. Optimization of appropriate resolution that can capture the relevant processes accurately for specific applications given computational resource constraints is also of great interest. GCHP
310 offers the unique global high resolution simulation capability, and also the opportunities to expand this analysis into a more comprehensive understanding of global resolution-dependence of NO_x and its nonlinear chemistry.

Author contributions. The manuscript was written through contributions of all authors. The conceptualization was initialized by CL, RVM and RCC. The methodology is developed by CL, LB and DZ. DC processed the satellite scattering weights. HW and JL conducted the offline emission calculation. CL performed the model simulations, visualization and analysis of the results. CL wrote the original draft. All authors have reviewed, edited, and given approval to the final version of the manuscript.

References

325 Beirle, S., Borger, C., Dörner, S., Li, A., Hu, Z., Liu, F., Wang, Y., and Wagner, T.: Pinpointing nitrogen oxide emissions from space, Science Advances, 5, eaax9800, https://doi.org/10.1126/sciadv.aax9800, _eprint: https://www.science.org/doi/pdf/10.1126/sciadv.aax9800, 2019.

Bey, I., Jacob, D. J., Yantosca, R. M., Logan, J. A., Field, B. D., Fiore, A. M., Li, Q., Liu, H. Y., Mickley, L. J., and Schultz, M. G.: Global modeling of tropospheric chemistry with assimilated meteorology: Model description and evaluation, Journal of Geophysical Research: Atmospheres, 106, 23 073–23 095, publisher: Wiley Online Library, 2001.

330 Bindle, L., Martin, R. V., Cooper, M. J., Lundgren, E. W., Eastham, S. D., Auer, B. M., Clune, T. L., Weng, H., Lin, J., Murray, L. T., Meng, J., Keller, C. A., Putman, W. M., Pawson, S., and Jacob, D. J.: Grid-stretching capability for the GEOS-Chem 13.0.0 atmospheric chemistry model, Geoscientific Model Development, 14, 5977–5997, https://doi.org/10.5194/gmd-14-5977-2021, 2021.

Brown, S. S. and Stutz, J.: Nighttime radical observations and chemistry, Chem. Soc. Rev., 41, 6405–6447, https://doi.org/10.1039/C2CS35181A, publisher: The Royal Society of Chemistry, 2012.

335 Brown, S. S., Neuman, J., Ryerson, T., Trainer, M., Dubé, W., Holloway, J., Warneke, C., De Gouw, J., Donnelly, S., and Atlas, E.: Nocturnal odd-oxygen budget and its implications for ozone loss in the lower troposphere, Geophysical research letters, 33, publisher: Wiley Online Library, 2006.

Browne, E. C. and Cohen, R. C.: Effects of biogenic nitrate chemistry on the NO_x lifetime in remote continental regions, Atmospheric Chemistry and Physics, 12, 11 917–11 932, https://doi.org/10.5194/acp-12-11917-2012, 2012.

340 Charlton-Perez, C. L., Evans, M. J., Marsham, J. H., and Esler, J. G.: The impact of resolution on ship plume simulations with NOx chemistry, Atmos. Chem. Phys., 9, 7505–7518, https://doi.org/10.5194/acp-9-7505-2009, publisher: Copernicus Publications, 2009.

Cooper, M., Martin, R. V., Padmanabhan, A., and Henze, D. K.: Comparing mass balance and adjoint methods for inverse modeling of nitrogen dioxide columns for global nitrogen oxide emissions, Journal of Geophysical Research: Atmospheres, 122, 4718–4734, publisher: Wiley Online Library, 2017.

345 Cooper, M. J., Martin, R. V., McLinden, C. A., and Brook, J. R.: Inferring ground-level nitrogen dioxide concentrations at fine spatial resolution applied to the TROPOMI satellite instrument, Environmental Research Letters, 15, 104 013, https://doi.org/10.1088/1748-9326/aba3a5, publisher: IOP Publishing, 2020.

Crippa, M., Guizzardi, D., Muntean, M., Schaaf, E., Dentener, F., van Aardenne, J. A., Monni, S., Doering, U., Olivier, J. G. J., Pagliari, V., and Janssens-Maenhout, G.: Gridded emissions of air pollutants for the period 1970–2012 within EDGAR v4.3.2, Earth System Science
350 Data, 10, 1987–2013, https://doi.org/10.5194/essd-10-1987-2018, 2018.

Crippa, M., Guizzardi, D., Muntean, M., and Schaaf, E.: EDGAR v5.0 Global Air Pollutant Emissions, http://data.europa.eu/89h/377801af-b094-4943-8fdc-f79a7c0c2d19, publisher: European Commission, 2021.

Eastham, S. D., Long, M. S., Keller, C. A., Lundgren, E., Yantosca, R. M., Zhuang, J., Li, C., Lee, C. J., Yannetti, M., Auer, B. M., Clune, T. L., Kouatchou, J., Putman, W. M., Thompson, M. A., Trayanov, A. L., Molod, A. M., Martin, R. V., and Jacob, D. J.: GEOS-Chem High
355 Performance (GCHP v11-02c): a next-generation implementation of the GEOS-Chem chemical transport model for massively \hack\break parallel applications, Geoscientific Model Development, 11, 2941–2953, https://doi.org/10.5194/gmd-11-2941-2018, 2018.

Edwards, P. M., Brown, S. S., Roberts, J. M., Ahmadov, R., Banta, R. M., deGouw, J. A., Dubé, W. P., Field, R. A., Flynn, J. H., Gilman, J. B., Graus, M., Helmig, D., Koss, A., Langford, A. O., Lefer, B. L., Lerner, B. M., Li, R., Li, S.-M., McKeen, S. A., Murphy, S. M., Parrish, D. D., Senff, C. J., Soltis, J., Stutz, J., Sweeney, C., Thompson, C. R., Trainer, M. K., Tsai, C., Veres, P. R., Washenfelder, R. A.,

360   Warneke, C., Wild, R. J., Young, C. J., Yuan, B., and Zamora, R.: High winter ozone pollution from carbonyl photolysis in an oil and gas
        basin, Nature, 514, 351–354, https://doi.org/10.1038/nature13767, 2014.

       Evans, M. and Jacob, D. J.: Impact of new laboratory studies of N2O5 hydrolysis on global model budgets of tropospheric nitrogen oxides,
        ozone, and OH, Geophysical Research Letters, 32, publisher: Wiley Online Library, 2005.

       Goldberg, D. L., Lu, Z., Streets, D. G., de Foy, B., Griffin, D., McLinden, C. A., Lamsal, L. N., Krotkov, N. A., and Eskes, H.: Enhanced
365   Capabilities of TROPOMI NO2: Estimating NOX from North American Cities and Power Plants, Environmental Science & Technology,
        53, 12 594–12 601, https://doi.org/10.1021/acs.est.9b04488, pMID: 31601103, 2019.

       Gu, B., Zhang, L., Van Dingenen, R., Vieno, M., Van Grinsven, H. J., Zhang, X., Zhang, S., Chen, Y., Wang, S., Ren, C., Rao, S., Holland, M.,
        Winiwarter, W., Chen, D., Xu, J., and Sutton, M. A.: Abating ammonia is more cost-effective than nitrogen oxides for mitigating PM2.5
        air pollution, Science, 374, 758–762, https://doi.org/10.1126/science.abf8623, publisher: American Association for the Advancement of
370   Science, 2021.

       Hoesly, R. M., Smith, S. J., Feng, L., Klimont, Z., Janssens-Maenhout, G., Pitkanen, T., Seibert, J. J., Vu, L., Andres, R. J., Bolt, R. M.,
        Bond, T. C., Dawidowski, L., Kholod, N., Kurokawa, J.-I., Li, M., Liu, L., Lu, Z., Moura, M. C. P., O'Rourke, P. R., and Zhang, Q.:
        Historical (1750–2014) anthropogenic emissions of reactive gases and aerosols from the Community Emissions Data System (CEDS),
        Geosci. Model Dev., 11, 369–408, https://doi.org/10.5194/gmd-11-369-2018, publisher: Copernicus Publications, 2018.

375   Holmes, C. D., Bertram, T. H., Confer, K. L., Graham, K. A., Ronan, A. C., Wirks, C. K., and Shah, V.: The role of clouds in the tropospheric
        NOx cycle: A new modeling approach for cloud chemistry and its global implications, Geophysical Research Letters, 46, 4980–4990,
        publisher: Wiley Online Library, 2019.

       Jacob, D. J., Horowitz, L. W., Munger, J. W., Heikes, B. G., Dickerson, R. R., Artz, R. S., and Keene, W. C.: Seasonal transition from NOx-
        to hydrocarbon-limited conditions for ozone production over the eastern United States in September, Journal of Geophysical Research:
380   Atmospheres, 100, 9315–9324, publisher: Wiley Online Library, 1995.

       Jin, X., Fiore, A. M., Murray, L. T., Valin, L. C., Lamsal, L. N., Duncan, B., Folkert Boersma, K., De Smedt, I., Abad, G. G., and Chance,
        K.: Evaluating a space-based indicator of surface ozone-NOx-VOC sensitivity over midlatitude source regions and application to decadal
        trends, Journal of Geophysical Research: Atmospheres, 122, 10–439, publisher: Wiley Online Library, 2017.

       Jin, X., Fiore, A., Boersma, K. F., Smedt, I. D., and Valin, L.: Inferring Changes in Summertime Surface Ozone–NOx–VOC Chem-
385   istry over U.S. Urban Areas from Two Decades of Satellite and Ground-Based Observations, Environ. Sci. Technol., 54, 6518–6529,
        https://doi.org/10.1021/acs.est.9b07785, publisher: American Chemical Society, 2020.

       Jung, J., Choi, Y., Mousavinezhad, S., Kang, D., Park, J., Pouyaei, A., Ghahremanloo, M., Momeni, M., and Kim, H.: Changes in the ozone
        chemical regime over the contiguous United States inferred by the inversion of NOx and VOC emissions using satellite observation,
        Atmospheric Research, 270, 106 076, https://doi.org/10.1016/j.atmosres.2022.106076, 2022.

390   Keller, C. A., Long, M. S., Yantosca, R. M., Da Silva, A. M., Pawson, S., and Jacob, D. J.: HEMCO v1.0: a versatile, ESMF-compliant com-
        ponent for calculating emissions in atmospheric models, Geoscientific Model Development, 7, 1409–1417, https://doi.org/10.5194/gmd-
        7-1409-2014, 2014.

       Kenagy, H. S., Sparks, T. L., Ebben, C. J., Wooldrige, P. J., Lopez-Hilfiker, F. D., Lee, B. H., Thornton, J. A., McDuffie, E. E., Fibiger, D. L.,
        and Brown, S. S.: NOx lifetime and NOy partitioning during WINTER, Journal of Geophysical Research: Atmospheres, 123, 9813–9827,
395   publisher: Wiley Online Library, 2018.

       Kim, J., Jeong, U., Ahn, M.-H., Kim, J. H., Park, R. J., Lee, H., Song, C. H., Choi, Y.-S., Lee, K.-H., Yoo, J.-M., Jeong, M.-J., Park,
        S. K., Lee, K.-M., Song, C.-K., Kim, S.-W., Kim, Y. J., Kim, S.-W., Kim, M., Go, S., Liu, X., Chance, K., Chan Miller, C., Al-Saadi, J.,

Veihelmann, B., Bhartia, P. K., Torres, O., Abad, G. G., Haffner, D. P., Ko, D. H., Lee, S. H., Woo, J.-H., Chong, H., Park, S. S., Nicks,
D., Choi, W. J., Moon, K.-J., Cho, A., Yoon, J., Kim, S.-k., Hong, H., Lee, K., Lee, H., Lee, S., Choi, M., Veefkind, P., Levelt, P. F.,
400   Edwards, D. P., Kang, M., Eo, M., Bak, J., Baek, K., Kwon, H.-A., Yang, J., Park, J., Han, K. M., Kim, B.-R., Shin, H.-W., Choi, H.,
Lee, E., Chong, J., Cha, Y., Koo, J.-H., Irie, H., Hayashida, S., Kasai, Y., Kanaya, Y., Liu, C., Lin, J., Crawford, J. H., Carmichael, G. R.,
Newchurch, M. J., Lefer, B. L., Herman, J. R., Swap, R. J., Lau, A. K. H., Kurosu, T. P., Jaross, G., Ahlers, B., Dobber, M., McElroy, C. T.,
and Choi, Y.: New Era of Air Quality Monitoring from Space: Geostationary Environment Monitoring Spectrometer (GEMS), Bulletin
of the American Meteorological Society, 101, E1–E22, https://doi.org/10.1175/BAMS-D-18-0013.1, place: Boston MA, USA Publisher:
405   American Meteorological Society, 2020.

Koplitz, S., Simon, H., Henderson, B., Liljegren, J., Tonnesen, G., Whitehill, A., and Wells, B.: Changes in Ozone Chemical Sensitivity in
the United States from 2007 to 2016, ACS Environ. Au, https://doi.org/10.1021/acsenvironau.1c00029, publisher: American Chemical
Society, 2021.

Koplitz, S. N., Mickley, L. J., Marlier, M. E., Buonocore, J. J., Kim, P. S., Liu, T., Sulprizio, M. P., DeFries, R. S., Jacob, D. J., Schwartz, J.,
410   Pongsiri, M., and Myers, S. S.: Public health impacts of the severe haze in Equatorial Asia in September–October 2015: demonstration
of a new framework for informing fire management strategies to reduce downwind smoke exposure, Environmental Research Letters, 11,
094 023, https://doi.org/10.1088/1748-9326/11/9/094023, 2016.

Lamsal, L., Martin, R., Van Donkelaar, A., Steinbacher, M., Celarier, E., Bucsela, E., Dunlea, E., and Pinto, J.: Ground-level nitrogen
dioxide concentrations inferred from the satellite-borne Ozone Monitoring Instrument, Journal of Geophysical Research: Atmospheres,
415   113, publisher: Wiley Online Library, 2008.

Larkin, A., Geddes, J. A., Martin, R. V., Xiao, Q., Liu, Y., Marshall, J. D., Brauer, M., and Hystad, P.: Global Land Use Regression Model
for Nitrogen Dioxide Air Pollution, Environ. Sci. Technol., 51, 6957–6964, https://doi.org/10.1021/acs.est.7b01148, publisher: American
Chemical Society, 2017.

Laughner, J. L. and Cohen, R. C.: Direct observation of changing NOx lifetime in North American cities, Science, 366, 723–727,
420   https://doi.org/10.1126/science.aax6832, publisher: American Association for the Advancement of Science, 2019.

Levelt, P. F., Joiner, J., Tamminen, J., Veefkind, J. P., Bhartia, P. K., Stein Zweers, D. C., Duncan, B. N., Streets, D. G., Eskes, H., van der
A, R., McLinden, C., Fioletov, V., Carn, S., de Laat, J., DeLand, M., Marchenko, S., McPeters, R., Ziemke, J., Fu, D., Liu, X., Pickering,
K., Apituley, A., González Abad, G., Arola, A., Boersma, F., Chan Miller, C., Chance, K., de Graaf, M., Hakkarainen, J., Hassinen, S.,
Ialongo, I., Kleipool, Q., Krotkov, N., Li, C., Lamsal, L., Newman, P., Nowlan, C., Suleiman, R., Tilstra, L. G., Torres, O., Wang, H.,
425   and Wargan, K.: The Ozone Monitoring Instrument: overview of 14 years in space, Atmospheric Chemistry and Physics, 18, 5699–5745,
https://doi.org/10.5194/acp-18-5699-2018, 2018.

Li, C., Martin, R. V., van Donkelaar, A., Boys, B. L., Hammer, M. S., Xu, J.-W., Marais, E. A., Reff, A., Strum, M., Ridley, D. A., Crippa, M.,
Brauer, M., and Zhang, Q.: Trends in Chemical Composition of Global and Regional Population-Weighted Fine Particulate Matter Esti-
mated for 25 Years, Environmental Science & Technology, 51, 11 185–11 195, https://doi.org/10.1021/acs.est.7b02530, pMID: 28891283,
430   2017.

Li, C., Zhu, Q., Jin, X., and Cohen, R. C.: Elucidating Contributions of Anthropogenic Volatile Organic Compounds and Particulate Matter
to Ozone Trends over China, Environmental Science & Technology, 56, 12 906–12 916, https://doi.org/10.1021/acs.est.2c03315, pMID:
36083302, 2022.

Lin, H., Jacob, D. J., Lundgren, E. W., Sulprizio, M. P., Keller, C. A., Fritz, T. M., Eastham, S. D., Emmons, L. K., Campbell, P. C.,
435   Baker, B., Saylor, R. D., and Montuoro, R.: Harmonized Emissions Component (HEMCO) 3.0 as a versatile emissions component for

14

atmospheric models: application in the GEOS-Chem, NASA GEOS, WRF-GC, CESM2, NOAA GEFS-Aerosol, and NOAA UFS models, Geoscientific Model Development, 14, 5487–5506, https://doi.org/10.5194/gmd-14-5487-2021, 2021.

Lin, J.-T. and McElroy, M. B.: Impacts of boundary layer mixing on pollutant vertical profiles in the lower troposphere: Implications to satellite remote sensing, Atmospheric Environment, 44, 1726–1739, https://doi.org/https://doi.org/10.1016/j.atmosenv.2010.02.009, 2010.

440 Long, M. S., Yantosca, R., Nielsen, J. E., Keller, C. A., da Silva, A., Sulprizio, M. P., Pawson, S., and Jacob, D. J.: Development of a grid-independent GEOS-Chem chemical transport model (v9-02) as an atmospheric chemistry module for Earth system models, Geoscientific Model Development, 8, 595–602, https://doi.org/10.5194/gmd-8-595-2015, 2015.

Lu, Z., Streets, D. G., de Foy, B., Lamsal, L. N., Duncan, B. N., and Xing, J.: Emissions of nitrogen oxides from US urban areas: estimation from Ozone Monitoring Instrument retrievals for 2005–2014, Atmospheric Chemistry and Physics, 15, 10367–10383,
445 https://doi.org/10.5194/acp-15-10367-2015, 2015.

Ma, X., Tan, Z., Lu, K., Yang, X., Chen, X., Wang, H., Chen, S., Fang, X., Li, S., Li, X., Liu, J., Liu, Y., Lou, S., Qiu, W., Wang, H., Zeng, L., and Zhang, Y.: OH and HO_2 radical chemistry at a suburban site during the EXPLORE-YRD campaign in 2018, Atmospheric Chemistry and Physics, 22, 7005–7028, https://doi.org/10.5194/acp-22-7005-2022, 2022.

Mao, J., Paulot, F., Jacob, D. J., Cohen, R. C., Crounse, J. D., Wennberg, P. O., Keller, C. A., Hudman, R. C., Barkley, M. P., and Horowitz,
450 L. W.: Ozone and organic nitrates over the eastern United States: Sensitivity to isoprene chemistry, Journal of Geophysical Research: Atmospheres, 118, 11–256, publisher: Wiley Online Library, 2013.

Martin, R. V., Sioris, C. E., Chance, K., Ryerson, T. B., Bertram, T. H., Wooldridge, P. J., Cohen, R. C., Neuman, J. A., Swanson, A., and Flocke, F. M.: Evaluation of space-based constraints on global nitrogen oxide emissions with regional aircraft measurements over and downwind of eastern North America, Journal of Geophysical Research: Atmospheres, 111, publisher: Wiley Online Library, 2006.

455 Martin, R. V., Eastham, S. D., Bindle, L., Lundgren, E. W., Clune, T. L., Keller, C. A., Downs, W., Zhang, D., Lucchesi, R. A., Sulprizio, M. P., Yantosca, R. M., Li, Y., Estrada, L., Putman, W. M., Auer, B. M., Trayanov, A. L., Pawson, S., and Jacob, D. J.: Improved Advection, Resolution, Performance, and Community Access in the New Generation (Version 13) of the High Performance GEOS-Chem Global Atmospheric Chemistry Model (GCHP), Geoscientific Model Development Discussions, 2022, 1–30, https://doi.org/10.5194/gmd-2022-42, 2022.

460 McDuffie, E. E., Fibiger, D. L., Dubé, W. P., Lopez-Hilfiker, F., Lee, B. H., Thornton, J. A., Shah, V., Jaeglé, L., Guo, H., and Weber, R. J.: Heterogeneous N2O5 uptake during winter: Aircraft measurements during the 2015 WINTER campaign and critical evaluation of current parameterizations, Journal of Geophysical Research: Atmospheres, 123, 4345–4372, publisher: Wiley Online Library, 2018.

Meng, J., Martin, R. V., Ginoux, P., Hammer, M., Sulprizio, M. P., Ridley, D. A., and van Donkelaar, A.: Grid-independent high-resolution dust emissions (v1.0) for chemical transport models: application to GEOS-Chem (12.5.0), Geoscientific Model Development, 14, 4249–
465 4260, https://doi.org/10.5194/gmd-14-4249-2021, 2021.

Miyazaki, K., Eskes, H., Sudo, K., Boersma, K. F., Bowman, K., and Kanaya, Y.: Decadal changes in global surface NO_x emissions from multi-constituent satellite data assimilation, Atmospheric Chemistry and Physics, 17, 807–837, https://doi.org/10.5194/acp-17-807-2017, 2017.

Murray, L. T., Jacob, D. J., Logan, J. A., Hudman, R. C., and Koshak, W. J.: Optimized regional and interannual variability of lightning in a
470 global chemical transport model constrained by LIS/OTD satellite data, Journal of Geophysical Research: Atmospheres, 117, publisher: Wiley Online Library, 2012.

Palmer, P. I., Jacob, D. J., Chance, K., Martin, R. V., Spurr, R. J. D., Kurosu, T. P., Bey, I., Yantosca, R., Fiore, A., and Li, Q.: Air mass factor formulation for spectroscopic measurements from satellites: Application to formaldehyde retrievals from the Global Ozone Monitoring

Experiment, Journal of Geophysical Research: Atmospheres, 106, 14 539–14 550, https://doi.org/https://doi.org/10.1029/2000JD900772,
475   _eprint: https://agupubs.onlinelibrary.wiley.com/doi/pdf/10.1029/2000JD900772, 2001.

Pan, S., Choi, Y., Roy, A., and Jeon, W.: Allocating emissions to 4 km and 1 km horizontal spatial resolutions and its impact on simulated
       NOx and O3 in Houston, TX, Atmospheric Environment, 164, 398–415, https://doi.org/10.1016/j.atmosenv.2017.06.026, 2017.

Perring, A. E., Pusede, S. E., and Cohen, R. C.: An Observational Perspective on the Atmospheric Impacts of Alkyl and Multifunctional
       Nitrates on Ozone and Secondary Organic Aerosol, Chem. Rev., 113, 5848–5870, https://doi.org/10.1021/cr300520x, publisher: American
480   Chemical Society, 2013.

Pusede, S. E., Steiner, A. L., and Cohen, R. C.: Temperature and Recent Trends in the Chemistry of Continental Surface Ozone, Chem. Rev.,
       115, 3898–3918, https://doi.org/10.1021/cr5006815, publisher: American Chemical Society, 2015.

Putman, W. M. and Lin, S.-J.: Finite-volume transport on various cubed-sphere grids, Journal of Computational Physics, 227, 55–78,
       https://doi.org/https://doi.org/10.1016/j.jcp.2007.07.022, 2007.

485   Qu, Z., Jacob, D. J., Silvern, R. F., Shah, V., Campbell, P. C., Valin, L. C., and Murray, L. T.: US COVID-19 shutdown demonstrates impor-
       tance of background NO2 in inferring NOx emissions from satellite NO2 observations, Geophysical research letters, 48, e2021GL092 783,
       publisher: Wiley Online Library, 2021.

Ren, X., Harder, H., Martinez, M., Lesher, R. L., Oliger, A., Simpas, J. B., Brune, W. H., Schwab, J. J., Demerjian, K. L., He, Y., Zhou,
       X., and Gao, H.: OH and HO2 Chemistry in the urban atmosphere of New York City, Atmospheric Environment, 37, 3639–3651,
490   https://doi.org/https://doi.org/10.1016/S1352-2310(03)00459-X, 2003.

Rollins, A. W., Browne, E. C., Min, K.-E., Pusede, S. E., Wooldridge, P. J., Gentner, D. R., Goldstein, A. H., Liu, S., Day,
       D. A., Russell, L. M., and Cohen, R. C.: Evidence for NOx Control over Nighttime SOA Formation, Science, 337, 1210–1212,
       https://doi.org/10.1126/science.1221520, publisher: American Association for the Advancement of Science, 2012.

Romer, P. S., Duffey, K. C., Wooldridge, P. J., Allen, H. M., Ayres, B. R., Brown, S. S., Brune, W. H., Crounse, J. D., de Gouw, J., Draper,
495   D. C., Feiner, P. A., Fry, J. L., Goldstein, A. H., Koss, A., Misztal, P. K., Nguyen, T. B., Olson, K., Teng, A. P., Wennberg, P. O., Wild,
       R. J., Zhang, L., and Cohen, R. C.: The lifetime of nitrogen oxides in an isoprene-dominated forest, Atmospheric Chemistry and Physics,
       16, 7623–7637, https://doi.org/10.5194/acp-16-7623-2016, 2016.

Romer Present, P. S., Zare, A., and Cohen, R. C.: The changing role of organic nitrates in the removal and transport of \chemNO_\mathitx,
       Atmospheric Chemistry and Physics, 20, 267–279, https://doi.org/10.5194/acp-20-267-2020, 2020.

500   Russell, A. R., Valin, L. C., and Cohen, R. C.: Trends in OMI NO$_2$ observations over the United States: effects of emission control technology
       and the economic recession, Atmospheric Chemistry and Physics, 12, 12 197–12 209, https://doi.org/10.5194/acp-12-12197-2012, 2012.

Shah, V., Jacob, D. J., Li, K., Silvern, R. F., Zhai, S., Liu, M., Lin, J., and Zhang, Q.: Effect of changing \chemNO_\mathitx lifetime on the
       seasonality and long-term trends of satellite-observed tropospheric \chemNO_2 columns over China, Atmospheric Chemistry and Physics,
       20, 1483–1495, https://doi.org/10.5194/acp-20-1483-2020, 2020.

505   Sherwen, T., Schmidt, J. A., Evans, M. J., Carpenter, L. J., Großmann, K., Eastham, S. D., Jacob, D. J., Dix, B., Koenig, T. K., Sinreich, R., Or-
       tega, I., Volkamer, R., Saiz-Lopez, A., Prados-Roman, C., Mahajan, A. S., and Ordóñez, C.: Global impacts of tropospheric halogens (Cl,
       Br, I) on oxidants and composition in GEOS-Chem, Atmospheric Chemistry and Physics, 16, 12 239–12 271, https://doi.org/10.5194/acp-
       16-12239-2016, 2016.

Sicard, P., De Marco, A., Agathokleous, E., Feng, Z., Xu, X., Paoletti, E., Rodriguez, J. J. D., and Calatayud, V.: Amplified ozone pollution in
510   cities during the COVID-19 lockdown, Science of The Total Environment, 735, 139 542, https://doi.org/10.1016/j.scitotenv.2020.139542,
       2020.

Sillman, S.: The relation between ozone, NOx and hydrocarbons in urban and polluted rural environments, Atmospheric Environment, 33, 1821–1845, https://doi.org/10.1016/S1352-2310(98)00345-8, 1999.

Sillman, S., Logan, J. A., and Wofsy, S. C.: A regional scale model for ozone in the United States with subgrid representation of urban and

515   power plant plumes, Journal of Geophysical Research: Atmospheres, 95, 5731–5748, publisher: Wiley Online Library, 1990.

Silvern, R. F., Jacob, D. J., Mickley, L. J., Sulprizio, M. P., Travis, K. R., Marais, E. A., Cohen, R. C., Laughner, J. L., Choi, S., Joiner, J., and Lamsal, L. N.: Using satellite observations of tropospheric \chemNO_2 columns to infer long-term trends in US \chemNO_\mathitx emissions: the importance of accounting for the free tropospheric \chemNO_2 background, Atmospheric Chemistry and Physics, 19, 8863–8878, https://doi.org/10.5194/acp-19-8863-2019, 2019.

520   Streets, D. G., Canty, T., Carmichael, G. R., de Foy, B., Dickerson, R. R., Duncan, B. N., Edwards, D. P., Haynes, J. A., Henze, D. K., Houyoux, M. R., Jacob, D. J., Krotkov, N. A., Lamsal, L. N., Liu, Y., Lu, Z., Martin, R. V., Pfister, G. G., Pinder, R. W., Salawitch, R. J., and Wecht, K. J.: Emissions estimation from satellite retrievals: A review of current capability, Atmospheric Environment, 77, 1011–1042, https://doi.org/10.1016/j.atmosenv.2013.05.051, 2013.

Thornton, J., Wooldridge, P., Cohen, R., Martinez, M., Harder, H., Brune, W., Williams, E., Roberts, J., Fehsenfeld, F., and Hall, S.: Ozone

525   production rates as a function of NOx abundances and HOx production rates in the Nashville urban plume, Journal of Geophysical Research: Atmospheres, 107, ACH–7, publisher: Wiley Online Library, 2002.

Timmermans, R., Segers, A., Curier, L., Abida, R., Attié, J.-L., El Amraoui, L., Eskes, H., de Haan, J., Kujanpää, J., Lahoz, W., Oude Nijhuis, A., Quesada-Ruiz, S., Ricaud, P., Veefkind, P., and Schaap, M.: Impact of synthetic space-borne \chemNO_2 observations from the Sentinel-4 and Sentinel-5P missions on tropospheric \chemNO_2 analyses, Atmospheric Chemistry and Physics, 19, 12 811–12 833,

530   https://doi.org/10.5194/acp-19-12811-2019, 2019.

Travis, K. R., Jacob, D. J., Fisher, J. A., Kim, P. S., Marais, E. A., Zhu, L., Yu, K., Miller, C. C., Yantosca, R. M., Sulprizio, M. P., Thompson, A. M., Wennberg, P. O., Crounse, J. D., St. Clair, J. M., Cohen, R. C., Laughner, J. L., Dibb, J. E., Hall, S. R., Ullmann, K., Wolfe, G. M., Pollack, I. B., Peischl, J., Neuman, J. A., and Zhou, X.: Why do models overestimate surface ozone in the Southeast United States?, Atmospheric Chemistry and Physics, 16, 13 561–13 577, https://doi.org/10.5194/acp-16-13561-2016, 2016.

535   Valin, L. C., Russell, A. R., Hudman, R. C., and Cohen, R. C.: Effects of model resolution on the interpretation of satellite NO2 observations, Atmos. Chem. Phys., 11, 11 647–11 655, https://doi.org/10.5194/acp-11-11647-2011, publisher: Copernicus Publications, 2011.

van der Werf, G. R., Randerson, J. T., Giglio, L., van Leeuwen, T. T., Chen, Y., Rogers, B. M., Mu, M., van Marle, M. J. E., Morton, D. C., Collatz, G. J., Yokelson, R. J., and Kasibhatla, P. S.: Global fire emissions estimates during 1997–2016, Earth System Science Data, 9, 697–720, https://doi.org/10.5194/essd-9-697-2017, 2017.

540   Veefkind, J., Aben, I., McMullan, K., Förster, H., de Vries, J., Otter, G., Claas, J., Eskes, H., de Haan, J., Kleipool, Q., van Weele, M., Hasekamp, O., Hoogeveen, R., Landgraf, J., Snel, R., Tol, P., Ingmann, P., Voors, R., Kruizinga, B., Vink, R., Visser, H., and Levelt, P.: TROPOMI on the ESA Sentinel-5 Precursor: A GMES mission for global observations of the atmospheric composition for climate, air quality and ozone layer applications, Remote Sensing of Environment, 120, 70–83, https://doi.org/10.1016/j.rse.2011.09.027, 2012.

Wang, J., Li, J., Ye, J., Zhao, J., Wu, Y., Hu, J., Liu, D., Nie, D., Shen, F., Huang, X., Huang, D. D., Ji, D., Sun, X., Xu, W., Guo, J.,

545   Song, S., Qin, Y., Liu, P., Turner, J. R., Lee, H. C., Hwang, S., Liao, H., Martin, S. T., Zhang, Q., Chen, M., Sun, Y., Ge, X., and Jacob, D. J.: Fast sulfate formation from oxidation of SO2 by NO2 and HONO observed in Beijing haze, Nature Communications, 11, 2844, https://doi.org/10.1038/s41467-020-16683-x, 2020.

Wang, K., Wu, K., Wang, C., Tong, Y., Gao, J., Zuo, P., Zhang, X., and Yue, T.: Identification of NOx hotspots from over-sampled TROPOMI NO2 column based on image segmentation method, Science of The Total Environment, 803, 150 007, https://doi.org/10.1016/j.scitotenv.2021.150007, 2022.

Wang, S., Ackermann, R., and Stutz, J.: Vertical profiles of O_3 and NO_x chemistry in the polluted nocturnal boundary layer in Phoenix, AZ: I. Field observations by long-path DOAS, Atmospheric Chemistry and Physics, 6, 2671–2693, https://doi.org/10.5194/acp-6-2671-2006, 2006.

Weng, H., Lin, J., Martin, R., Millet, D. B., Jaeglé, L., Ridley, D., Keller, C., Li, C., Du, M., and Meng, J.: Global high-resolution emissions of soil NOx, sea salt aerosols, and biogenic volatile organic compounds, Scientific Data, 7, 148, https://doi.org/10.1038/s41597-020-0488-5, 2020.

Wild, O. and Prather, M. J.: Global tropospheric ozone modeling: Quantifying errors due to grid resolution, Journal of Geophysical Research: Atmospheres, 111, https://doi.org/https://doi.org/10.1029/2005JD006605, 2006.

Yamaji, K., Ikeda, K., Irie, H., Kurokawa, J., and Ohara, T.: Influence of model grid resolution on NO2 vertical column densities over East Asia, null, 64, 436–444, https://doi.org/10.1080/10962247.2013.827603, publisher: Taylor & Francis, 2014.

Yan, Y., Lin, J., Chen, J., and Hu, L.: Improved simulation of tropospheric ozone by a global-multi-regional two-way coupling model system, Atmospheric Chemistry and Physics, 16, 2381–2400, https://doi.org/10.5194/acp-16-2381-2016, 2016.

Yan, Y., Lin, J., and He, C.: Ozone trends over the United States at different times of day, Atmospheric Chemistry and Physics, 18, 1185–1202, https://doi.org/10.5194/acp-18-1185-2018, 2018.

Yu, K., Jacob, D. J., Fisher, J. A., Kim, P. S., Marais, E. A., Miller, C. C., Travis, K. R., Zhu, L., Yantosca, R. M., Sulprizio, M. P., Cohen, R. C., Dibb, J. E., Fried, A., Mikoviny, T., Ryerson, T. B., Wennberg, P. O., and Wisthaler, A.: Sensitivity to grid resolution in the ability of a chemical transport model to simulate observed oxidant chemistry under\hack\break high-isoprene conditions, Atmospheric Chemistry and Physics, 16, 4369–4378, https://doi.org/10.5194/acp-16-4369-2016, 2016.

Zakoura, M. and Pandis, S.: Overprediction of aerosol nitrate by chemical transport models: The role of grid resolution, Atmospheric Environment, 187, 390–400, https://doi.org/10.1016/j.atmosenv.2018.05.066, 2018.

Zhang, R., Lei, W., Tie, X., and Hess, P.: Industrial emissions cause extreme urban ozone diurnal variability, Proceedings of the National Academy of Sciences, 101, 6346–6350, https://doi.org/10.1073/pnas.0401484101, publisher: Proceedings of the National Academy of Sciences, 2004.

Zhu, Q., Laughner, J. L., and Cohen, R. C.: Lightning \chemNO_2 simulation over the contiguous US and its effects on satellite \chemNO_2 retrievals, Atmospheric Chemistry and Physics, 19, 13 067–13 078, https://doi.org/10.5194/acp-19-13067-2019, 2019.

Zhu, Q., Laughner, J. L., and Cohen, R. C.: Estimate of OH trends over one decade in North American cities, Proceedings of the National Academy of Sciences, 119, e2117399 119, https://doi.org/10.1073/pnas.2117399119, publisher: Proceedings of the National Academy of Sciences, 2022.

Zoogman, P., Liu, X., Suleiman, R., Pennington, W., Flittner, D., Al-Saadi, J., Hilton, B., Nicks, D., Newchurch, M., Carr, J., Janz, S., Andraschko, M., Arola, A., Baker, B., Canova, B., Chan Miller, C., Cohen, R., Davis, J., Dussault, M., Edwards, D., Fishman, J., Ghu-lam, A., González Abad, G., Grutter, M., Herman, J., Houck, J., Jacob, D., Joiner, J., Kerridge, B., Kim, J., Krotkov, N., Lamsal, L., Li, C., Lindfors, A., Martin, R., McElroy, C., McLinden, C., Natraj, V., Neil, D., Nowlan, C., OSullivan, E., Palmer, P., Pierce, R., Pippin, M., Saiz-Lopez, A., Spurr, R., Szykman, J., Torres, O., Veefkind, J., Veihelmann, B., Wang, H., Wang, J., and Chance, K.: Tropospheric emissions: Monitoring of pollution (TEMPO), Journal of Quantitative Spectroscopy and Radiative Transfer, 186, 17–39, https://doi.org/10.1016/j.jqsrt.2016.05.008, 2017.
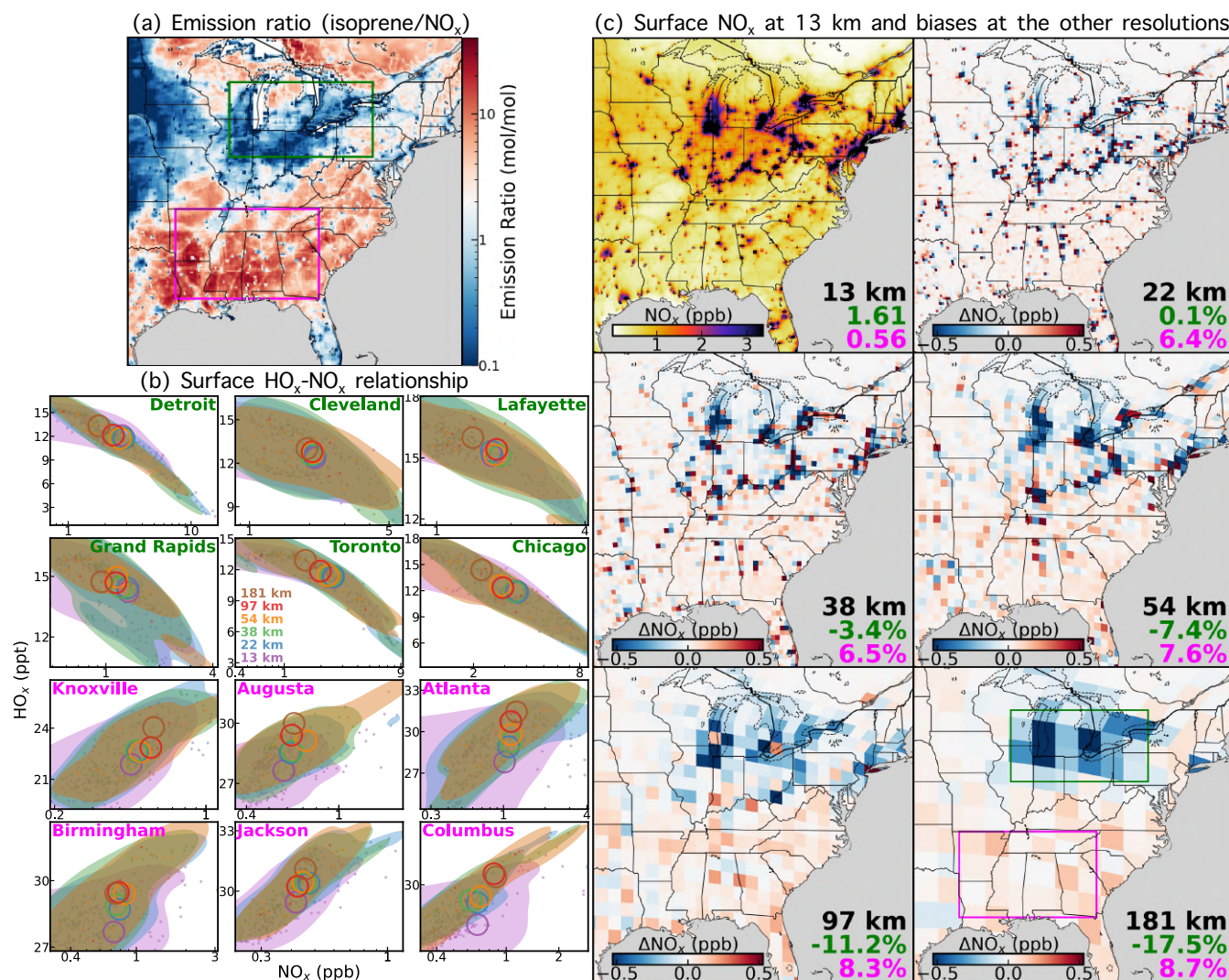
Figure 1. Daytime (UTC 15-24 or CST 9-18) resolution effects of surface NO_x concentration driven by NO_x-HO_x feedbacks (e.g., Figure S1) over July, 2015. (a) Emission ratio of isoprene vs. NO_x; (b) Simulated HO_x-NO_x relationship at each resolution (color-coded). The contour lines (for resolutions < 60 km) include 90% of the 2-d scatter (points) of data within 2°×2° window centered over each city (based on kernel density estimation), and the circles place the means for all resolutions; (c) Surface NO_x concentration at 13 km (top left) and the differences (minus 13 km) at the other resolutions (other panels). The regional mean NO_x (for 13 km, in ppb) and percentage biases (for the other resolutions) are indicated at the bottom right of each panel. Green and magenta (rectangles, city names and numbers) label the Great Lakes region and Southern States, respectively.
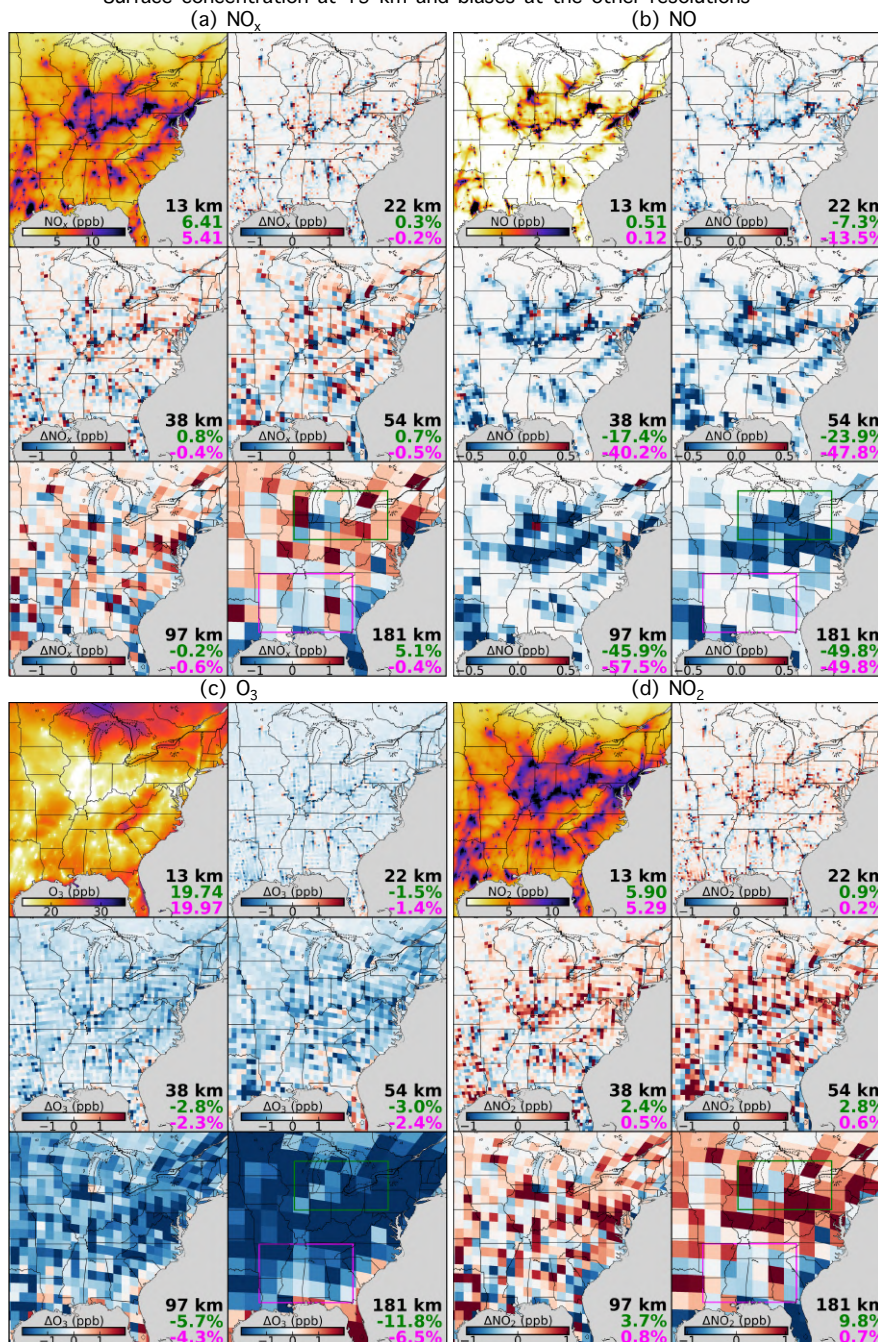
Figure 2. **Nighttime (UTC 4-11 or CST 22-5) resolution effects of surface** NO_x **concentration driven by** NO **titration of** O_3 (e.g., Figure S6) during January, 2015. Each panel is similar to Figure 1c but for nighttime surface concentrations of (a) NO_x, (b) NO, (c) O_3, and (d) NO_2.
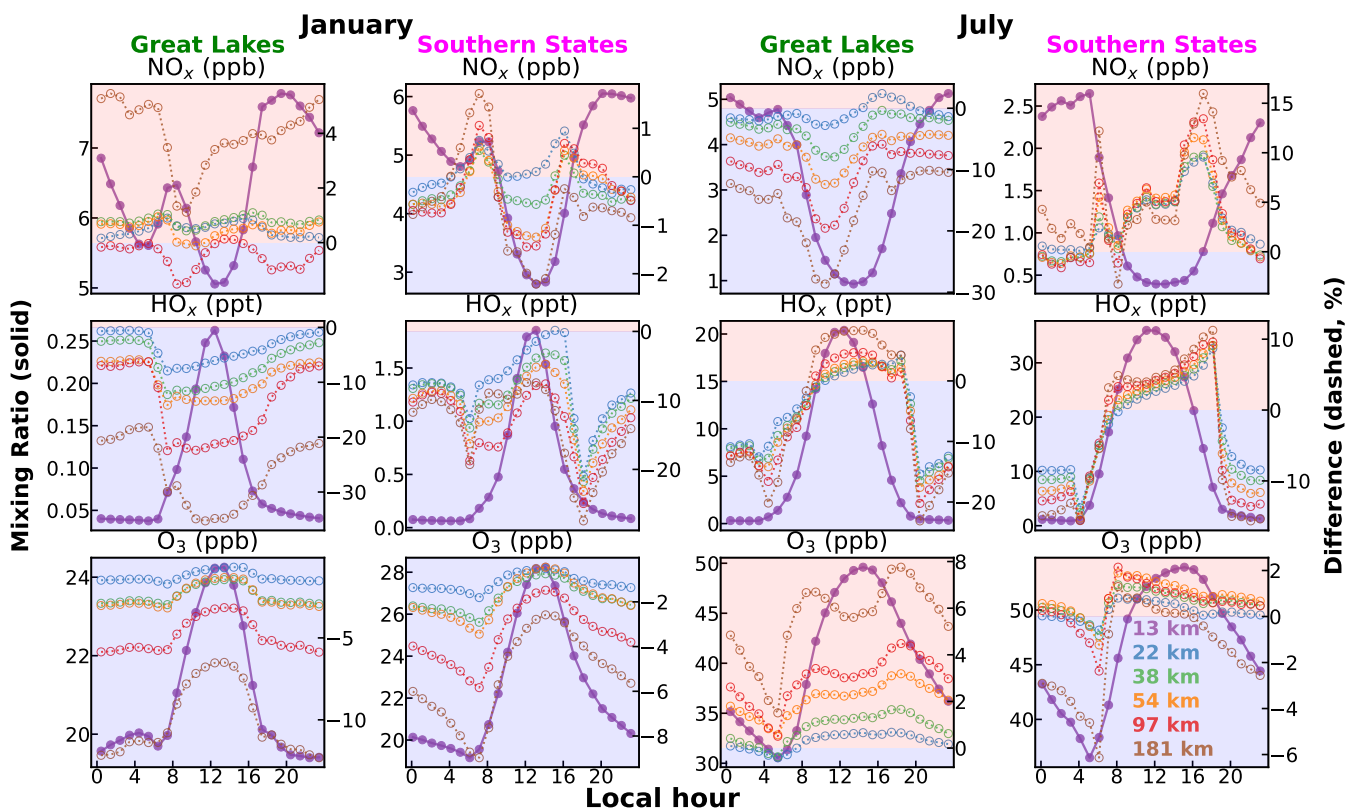
Figure 3. Resolution effects of surface NO_x **dominated by nighttime biases in January and by daytime biases in July**, 2015. The absolute monthly mixing ratios (left Y-axis) of regional mean NO_x, HO_x and O_3 are shown as filled symbols and solid lines at 13 km resolution, and the differences vs. 13 km (right Y-axis) are shown as empty symbols and dashed lines for the other resolutions (see color-legends). The positive (light red) and negative (light blue) difference regimes are color-divided.
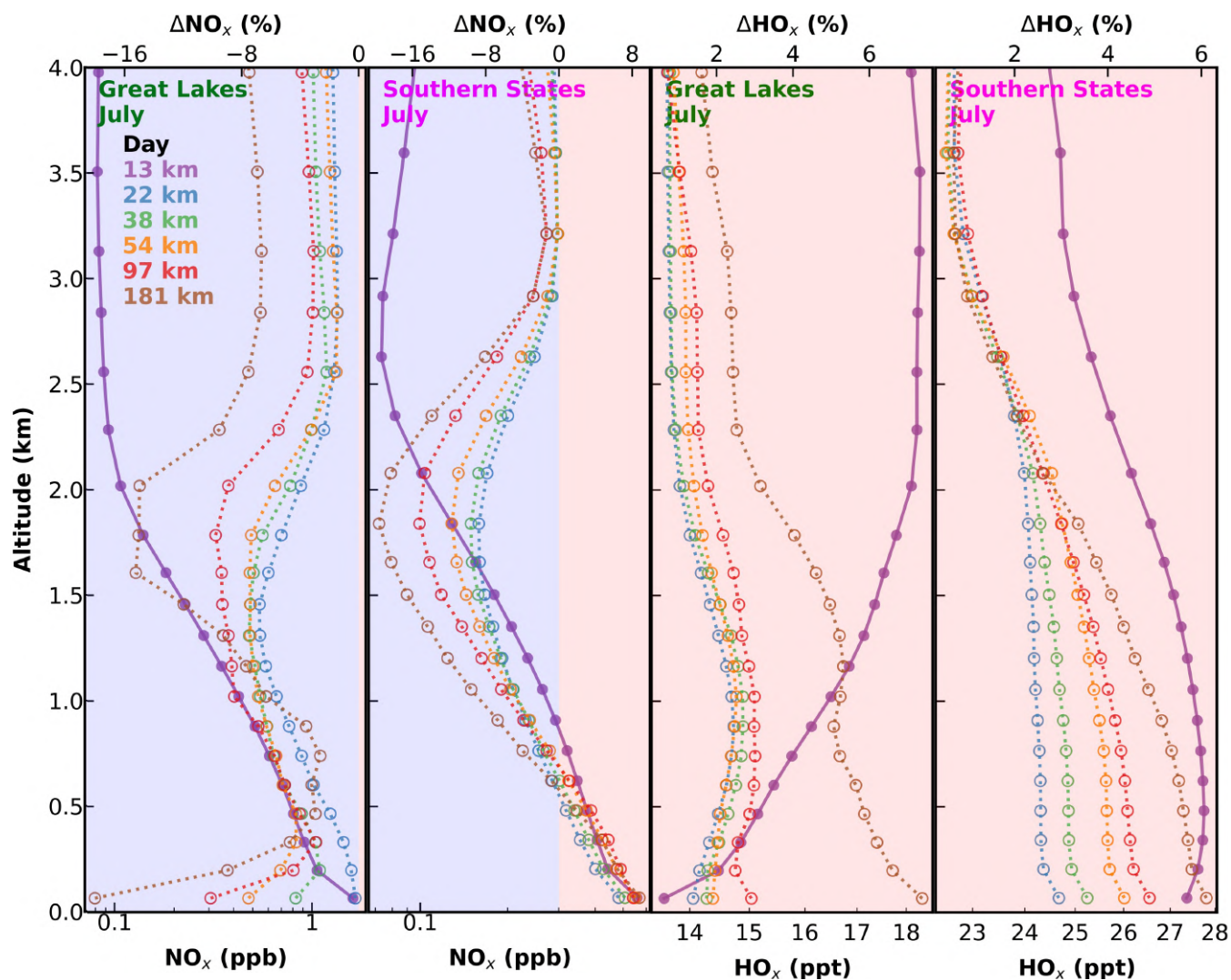
Figure 4. Change of daytime NO_x **vertical distribution in the lower troposphere at different resolutions** in July. The absolute monthly and regional mean concentrations (lower-X axis) of NO_x and HO_x are shown as filled symbols and solid lines at 13 km resolution, and the differences vs. 13 km (upper-X axis) is shown as empty symbols and dashed lines for the other resolutions (see color-legends). The positive (light red) and negative (light blue) difference regimes are color-divided.
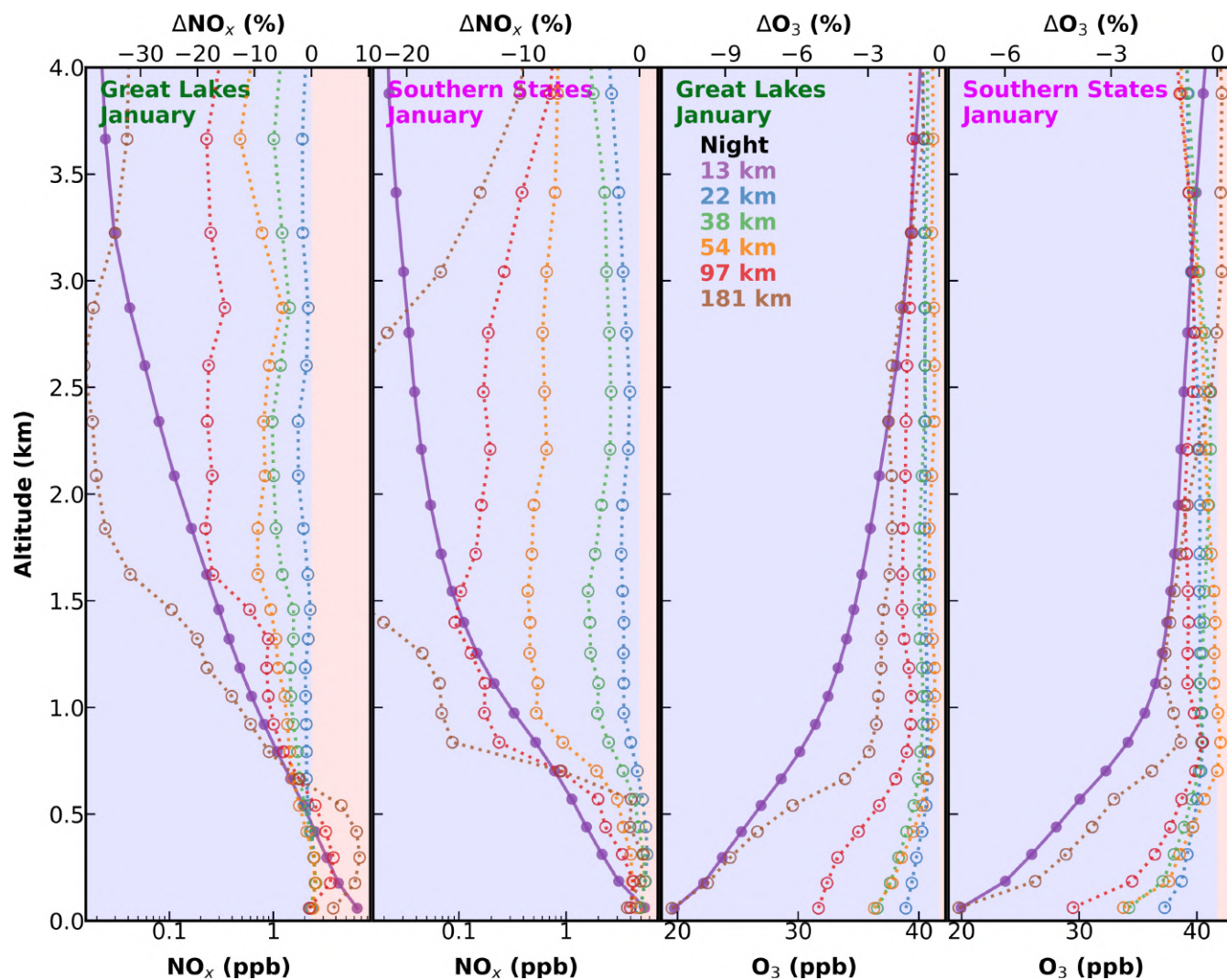
Figure 5. Change of nighttime NO_x vertical distribution in the lower troposphere at different resolutions in January. Similar to Figure 4 but for nighttime NO_x and O_3 in January.

Fraction of tropospheric NO_2 column within the surface layer at 13 km and biases at the other resolutions
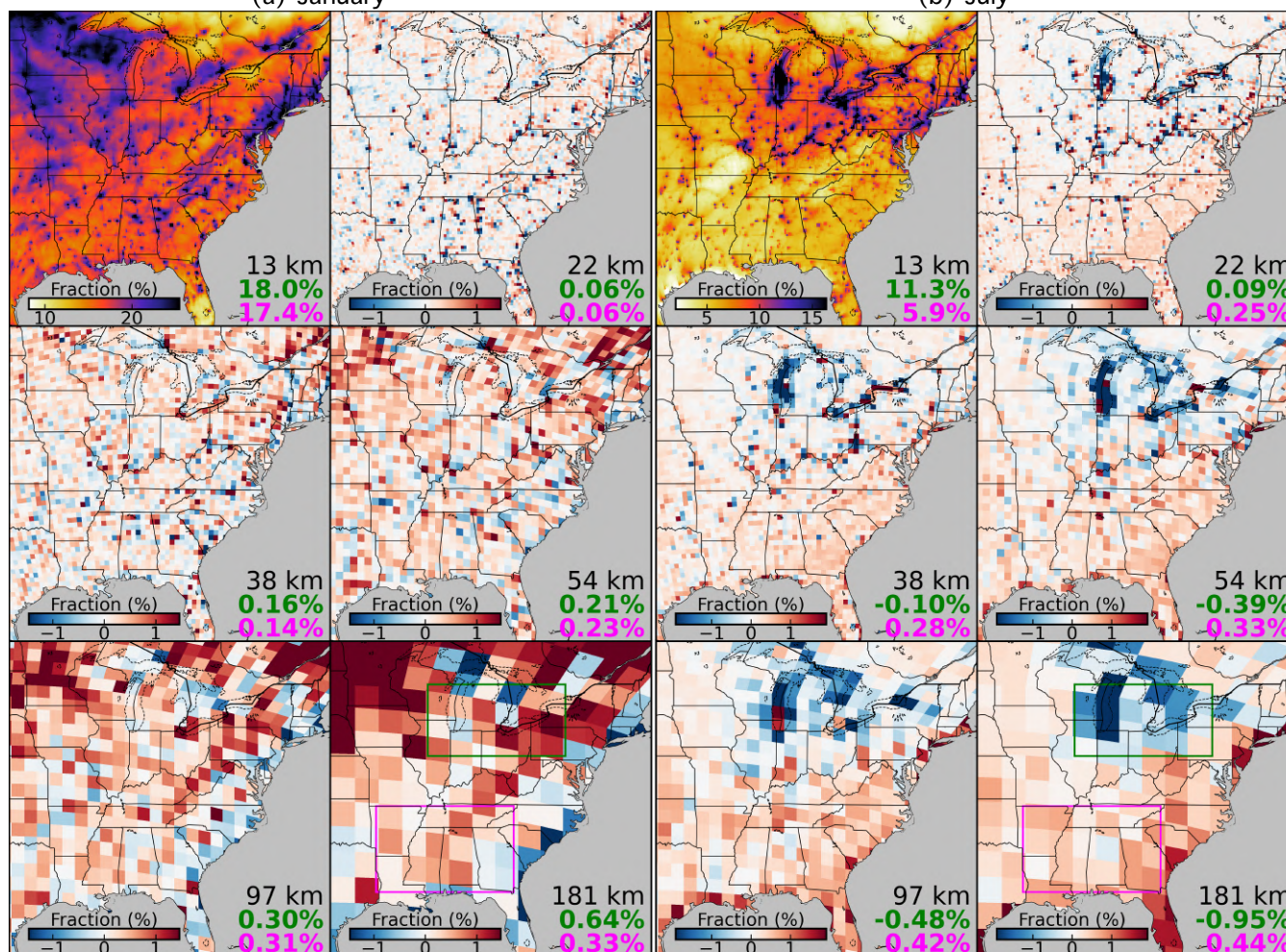
(a) January   (b) July

Figure 6. Coarse resolution simulations yield variable biases in satellite-based estimation of surface NO_2 concentration. Panels (a) and (b) are both similar to Figure 1c (for January and July, 2015, respectively) but for the fraction (%) of NO_2 tropospheric column within the surface layer during afternoon satellite overpass time (UTC 19-21). The numbers for the other resolutions vs. 13 km are absolute differences in percentage number.

Tropospheric NO$_2$ column density at 13 km and biases at the other resolutions
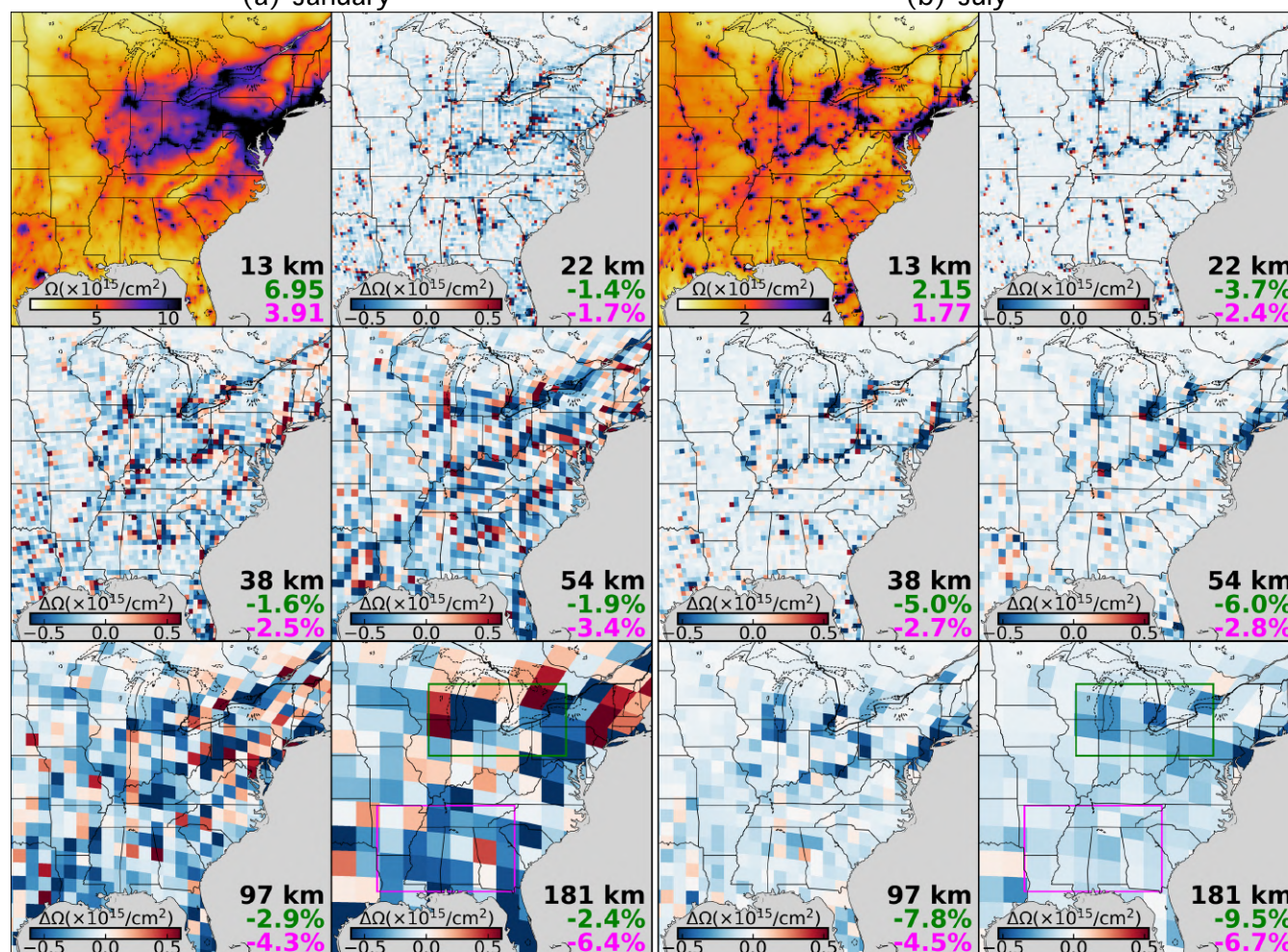(a) January   (b) July

Figure 7. Coarse resolution simulations yield positive biases in spaceborne inverse modeling of NO$_x$ emissions. Panels (a) and (b) are both similar to Figure 1c (for January and July, 2015, respectively) but for the mean GEOS-Chem tropospheric NO$_2$ column density (in molecules/cm^2) during afternoon satellite overpass time (UTC 19-21).

Table 1. Description of the simulations with six resolutions over the eastern US.

Cubed-sphere grids[a]	Stretch factor[b]	Center of the refined domain	Average resolution in the eastern US (km)
C48			181
C90	N/A	N/A	97
C160			54
C100	2.8		38
C136	3.5	37°N, 84°W	22
C180	4.3		13

[a] A cubed-sphere grid contains a mosaic of six grids (faces). Each face is regularly spaced with N×N grid cells, and the notation of each resolution (CN) here identifies the size N.

[b] Stretch factor (S) defines the strength of the grid-stretching. The resolution is about S times higher than the regular cubed-sphere over the refined region (eastern US), while is about 1/S of the original resolution over the antipode.